https://doi.org/10.5194/tc-2020-357
Preprint. Discussion started: 21 January 2021

The Cryosphere
Discussions
Open Access

A local model of snow-firn dynamics and application to Colle Gnifetti site

Fabiola Banfi[1] and Carlo De Michele[1]

[1]Department of Civil and Environmental Engineering, Politecnico di Milano, Milano, Italy

Correspondence: Fabiola Banfi (fabiola.banfi@polimi.it), Carlo De Michele (carlo.demichele@polimi.it)

Abstract. The regulating role of glaciers on catchment run-off is of fundamental importance in sustaining people living in low lying areas. The reduction in glacierized areas under the effect of climate change disrupts the distribution and amount of run-off, threatening water supply, agriculture and hydropower. The prediction of these changes requires models that integrate hydrological, nivological and glaciological processes. In this work we propose a local model that combines the nivological and glaciological scales, developed with the aim of a subsequent integration in hydrological distributed models. The model was derived from mass balance, momentum balance and rheological equations and describes the formation and evolution of the snowpack and the firn below it. The model was applied at the site of Colle Gnifetti (Monte Rosa massif, 4400–4550 $\mathrm{m\,a.s.l.}$). We obtained an average net accumulation of $0.26 \cdot 10^3\ \mathrm{kg\,m^{-2}\,y^{-1}}$ to be compared with the observed net annual accumulation that increases from about $0.15 \cdot 10^3\ \mathrm{kg\,m^{-2}\,y^{-1}}$ to about $1.2 \cdot 10^3\ \mathrm{kg\,m^{-2}\,y^{-1}}$ moving from the north facing to the south facing slope. The model results confirm the strong influence of wind on snow accumulation and densification, observed also from ice cores. The conserved precipitation is made up mainly of snow deposited between May and September, when temperatures above melting point are also observed. Even though the variability of annual snow accumulation is not well reproduced by the model, the modelled and observed firn densities show a good agreement up to the depth reached by the model with the available input data.

1 Introduction

Glacier ice covers almost 16 million $\mathrm{km^2}$ of the Earth's surface, of which it is estimated that only 3 % is retained by the mountains outside the polar region (Benn and Evans, 2010). Despite this small percentage the amount of water stored in mountain glaciers plays a key role in sustaining people living in low lying areas (Adhikary, 1993), influencing run-off on a wide range of temporal and spatial scales (Jansson et al., 2003; Huss et al., 2010). Storing water coming from precipitation in winter and delaying the time in which it reaches the river network, they sustain streamflow in hotter and drier periods when precipitation is lacking and when it is most needed for agriculture and as drinking water (Fountain and Tangborn, 1985; Hagg et al., 2007). Jost et al. (2012) found in upper Columbia river basin (Canada) covered for only 5 % by glaciers, that ice melt contributes up to 25 % and 35 % to streamflow respectively in August and September and between 3 % and 9 % to total streamflow. In high mountain river basins of the northern Tien Shan (Central Asia), with areas of glaciation higher than

https://doi.org/10.5194/tc-2020-357
Preprint. Discussion started: 21 January 2021

30–40 %, glaciermelt contribution is 18–28 % of annual run-off but it can increase to 40–70 % during summer (Aizen et al., 1996).

The reduction of glacier volume observed over the past 150 years (Vaughan et al., 2013; Hock et al., 2019) will result in a change in the present distribution and amount of water storage and release with implications in all aspects of watershed management (Hock et al., 2005) with consequent high economic impacts (Huss et al., 2010). The prediction of these changes is therefore fundamental in order to asses and reduce their impacts, optimizing consequently the management of water resources. To accomplish this task, models that integrate hydrological, nivological and glaciological components and that consider a variable glacier extension and the transient response of glacier to climate change are required (Luo et al., 2013).

Despite their importance, fully integrated glacio-hydrological catchment models are not common in literature (Wortmann et al., 2019). A keyword search in Scopus carried out the 7^{th} of August 2020 produced 21803 results using only the keyword "hydrological modelling" that reduced to 288 adding the keyword "glacier". The combination of "hydrological modelling" and "glacier mass balance" produced 65 results and the combination of "hydrological modelling" with "glacier mass balance" and "glacier dynamics" 11 results. Some examples of glacio-hydrological models are provided by the works of Huss et al. (2010); Naz et al. (2014); Seibert et al. (2018) and Wortmann et al. (2019).

Wortmann et al. (2019) grouped the main problems of glacio-hydrological models in two categories: integration and scale. With integration problems they refer to the simplified or absent description of the remaining catchment hydrology in models that describe in detail glacier processes. The decrease in the fraction of ice covered areas requires a proper description of both components also in basins that in the present are highly glacierized. Another aspect is the integration of nivological and glaciological components: a joint simulation of glacier mass balance and snow accumulation and melt is required in order to avoid inconsistencies (Jost et al., 2012; Naz et al., 2014). The problems of scale arise from the different resolutions required by glacial, nivological and hydrological processes. Physically based models that consider all glacier processes (mass balance, subglacial drainage and ice flow dynamics) are often too computationally expensive to be used in a combined glacio-hydrological model that considers the entire catchment. In addition they are characterized by a complexity higher than the one of many semi-distributed hydrological models. It is therefore necessary to develop glacier models with a degree of complexity similar to the one of hydrological models but that are still able to reproduce the important processes (Seibert et al., 2018).

In the present work we give our contribution proposing a local model that integrates the nivological and glaciological components and that could be potentially integrated in a hydrological model. The model follows the transformation of snow into firn and glacier ice under the influence of temperature, precipitation and wind speed. It consists of six differential equations derived from mass balance, momentum balance and rheological equations that estimate the snowpack and firn characteristics (depth and density of snow and firn, depth of water and ice inside the snowpack). The equations that describe the snowpack are derived from the work of De Michele et al. (2013) and later Avanzi et al. (2015), modified in order to take into account the contribution of wind erosion and the mass exchange between snow and firn. To model the firn component, the densification model proposed by Arnaud et al. (2000) was used. In order to test the model a high altitude site, Colle Gnifetti, belonging to the Monte Rosa massif was chosen. Due to the lack of precipitation data a simple procedure to reconstruct them using two lower altitude stations is also proposed.

https://doi.org/10.5194/tc-2020-357
Preprint. Discussion started: 21 January 2021

The manuscript is organized in the following way: we provide the model in Sec. 2; illustrate the case study in Sec. 3; give the results in Sec. 4 and discussion in Sec. 5. The conclusions are given in Sec. 6.

2 Methodology

In this section, firstly the snowpack model, proposed by De Michele et al. (2013) and later modified by Avanzi et al. (2015), with the addition of the contribution of wind to snow transport is illustrated and secondly the model with the integration of snow and firn processes is presented.

2.1 Snow model

The snowpack is modelled, according to De Michele et al. (2013) and Avanzi et al. (2015), as a mixture of dry and wet constituents. The solid deformable skeleton, composed by snow grains and pores, has a total volume V_S with unitary area, height h_S, mass M_S and density ρ_S. The liquid water inside the pores has a volume V_W with unitary area, height h_W, mass M_W and constant density $\rho_W = 1000\ \mathrm{kg\,m^{-3}}$. The iced water inside the pores due to refreezing has a volume V_{MF} with unitary area, height h_{MF}, mass M_{MF} and constant density $\rho_i = 917\ \mathrm{kg\,m^{-3}}$. It is also possible to define the bulk snow density (ρ), snow water equivalent (SWE) and volumetric liquid water content (θ_W) as $\rho = (\rho_S h_S + \rho_W h_W + \rho_i h_{MF})/h$, $SWE = (\rho h)/\rho_W$ and $\theta_W = h_W/h$ where h is the height of the snowpack equal to $h = h_S + \langle h_{MF} + h_W - \phi h_S \rangle$ (Avanzi et al., 2015) in which $\langle\rangle$ are the Macaulay brackets that provide the argument if this is positive and zero otherwise and ϕ is the porosity.

The model solves the mass balance for the dry and liquid mass of the snowpack and the momentum balance and rheological equation for the solid deformable skeleton, resulting in four Ordinary Differential Equations (ODEs) in the variables h_S, h_W, h_{MF} and ρ_S. The mass fluxes considered are (1) solid precipitation events, snow melt and wind erosion for the dry snow mass, (2) rain events, snow melt, melt-freeze inside the snowpack and run-off for the liquid mass and (3) melt-freeze for the mass of ice. The dry snow density is obtained considering (1) a densification due to overburden stress, (2) a densification due to drifting snow compaction and (3) a densification due to addition of new mass. Accordingly, the following system is obtained (see Appendix A for the derivation of the system and the detailed description of the terms in the equations):

$$\frac{dh_S}{dt} = -\frac{h_S}{\rho_S}\frac{d\rho_S}{dt} + \frac{\rho_{NS}}{\rho_S}s - (I \cdot a)(T_A - T_\tau) - \frac{Q}{\rho_S} \tag{1a}$$

$$\frac{dh_W}{dt} = r + \frac{\rho_S}{\rho_W}(I \cdot a)(T_A - T_\tau) + (I^* \cdot e \cdot a)(T_A - T_\tau) - \alpha \cdot K_W \tag{1b}$$

$$\frac{dh_{MF}}{dt} = -\frac{\rho_W}{\rho_i}(I^* \cdot e \cdot a)(T_A - T_\tau) \tag{1c}$$

$$\frac{d\rho_S}{dt} = (c \cdot A_1 \cdot U)\rho_S \exp(-B \cdot (T_\tau - T_S) - A_2 \cdot \rho_S) + \frac{\rho_{NS} - \rho_S}{h_S}s \tag{1d}$$

In Eq. (1a), ρ_{NS} is the density of fresh snow ($\mathrm{kg\,m^{-3}}$), s is the solid precipitation rate ($\mathrm{m\,h^{-1}}$), a is a calibration parameter ($\mathrm{m\,h^{-1}\,{}^\circ C^{-1}}$), T_A and T_τ are the air temperature and the threshold temperature for melting ($^\circ\mathrm{C}$), I is the product of a binary

https://doi.org/10.5194/tc-2020-357
Preprint. Discussion started: 21 January 2021

function equal to 1 if $T_A \geq T_\tau$ and of a function of h_S, namely $\frac{h_S}{h_S+k}$, which tends to 0 with h_S, with $k = 0.01$ m (Avanzi et al., 2015) and Q is the mass of snow eroded by wind ($\mathrm{kg\,m^{-2}\,h^{-1}}$). In Eq. (1b), r is the liquid precipitation rate ($\mathrm{m\,h^{-1}}$), e is a calibration parameter, I^* is equal to $\frac{h_W}{h_W+k}$ if $T_A < T_\tau$ and to $\frac{h_{MF}}{h_{MF}+k}$ if $T_A > T_\tau$ (Avanzi et al., 2015), $\alpha = 1.9692 \cdot 10^9\ \mathrm{m^{-1}\,h^{-1}}$ (DeWalle and Rango, 2008) and K_W is the intrinsic permeability of water in snow ($\mathrm{m^2}$). In Eq. (1d), $c = 0.10 \cdot 3600\ \mathrm{s\,h^{-1}}$, $A_1 = 0.0013\ \mathrm{m^{-1}}$, $A_2 = 0.021\ \mathrm{m^3\,kg^{-1}}$, $B = 0.08\ \mathrm{K^{-1}}$ (Liston et al., 2007), U is the wind speed contribution ($\mathrm{m\,s^{-1}}$) and T_S is the average snow temperature (°C) obtained assuming thermal equilibrium between the constituents and a bilinear profile of temperature through depth (see De Michele et al. (2013) for further details).

With respect to the model by De Michele et al. (2013) and Avanzi et al. (2015), the version presented in this work includes the effect of wind both on mass balance and densification. This is important when the model is applied to high altitude sites: Haeberli and Alean (1985), in fact, suggested that a major part of the decrease of accumulation with altitude in the Alps, that occurs above about 3500 m a.s.l., may be due to wind effects.

In analogy with solid transport, snow is mobilized only when wind velocity at the surface exceeds a given threshold that depends on physical proprieties of the surface snowpack (Li and Pomeroy, 1997). Once transport begins, snow can travel in two main modes: saltation and suspension (Déry and Taylor, 1996; Pomeroy et al., 1997).

The total snow transport Q is computed by the model with the following assumptions: (1) only snow erosion occurs and no deposition of snow eroded in other positions is present; (2) measured wind speed is always referred to 10 m height, i.e. the height of the snow on the ground is neglected; (2) wind cannot erode snow that experienced a temperature greater than 0 °C for the presence of ice crusts or wet layers following Vionnet et al. (2018). These last two assumptions allow to compute the series of total snow transport Q decoupled from the snow model since knowledge of snow height is not required.

To implement the routine, we proceeded as explained in the following. When the first solid precipitation event occurs in a time step, the amount of new snow on the ground at the end of the time step, S_A ($\mathrm{kg\,m^{-2}\,h^{-1}}$), is obtained subtracting from the mass of solid precipitation the snow transport calculated for that time step, where snow transport is zero if the wind speed is lower than the threshold wind speed. This value is saved along with the time of deposition and ρ_{NS} of the event. During the subsequent steps, the threshold is recomputed updating the average temperature and the time since deposition and the theoretical snow transport for the time step is obtained. The actual snow transport is then obtained considering four different situations: (1) a new snow event occurs in the time step. In this case S_A is moved into a vector $\boldsymbol{S_R}$ with its time of deposition and ρ_{NS}. If $Q < \rho_{NS} \cdot s$ then S_A is recomputed as $\rho_{NS} \cdot s - Q$, vice versa previously deposited events are eroded as in step (4); (2) $T_A > 0$ °C. In this case S_A and Q are set to 0 $\mathrm{kg\,m^{-2}\,h^{-1}}$ and all the old snow events memorized in $\boldsymbol{S_R}$ are removed; (3) $T_A < 0$ °C and $Q < S_A$. In this case S_A is set to $S_A = S_A - Q$; (4) $T_A < 0$ °C and $Q > S_A$. In this case, if $\boldsymbol{S_R}$ has no elements, Q is set equal to S_A and S_A to 0 $\mathrm{kg\,m^{-2}\,h^{-1}}$, otherwise the difference between Q and S_A is subtracted from the most recent event in $\boldsymbol{S_R}$, given that wind speed is higher than the threshold recomputed with the characteristics of that event, and this event is removed from $\boldsymbol{S_R}$. This is repeated until an event in $\boldsymbol{S_R}$ that cannot be eroded by wind is encountered or the total amount of snow eroded in that time step reaches Q. In the latter case the actual transport is Q while in the former Q is given by the total amount of snow eroded before reaching the non erodible layer. The new S_A is the amount of snow associated with the last event considered.

https://doi.org/10.5194/tc-2020-357
Preprint. Discussion started: 21 January 2021

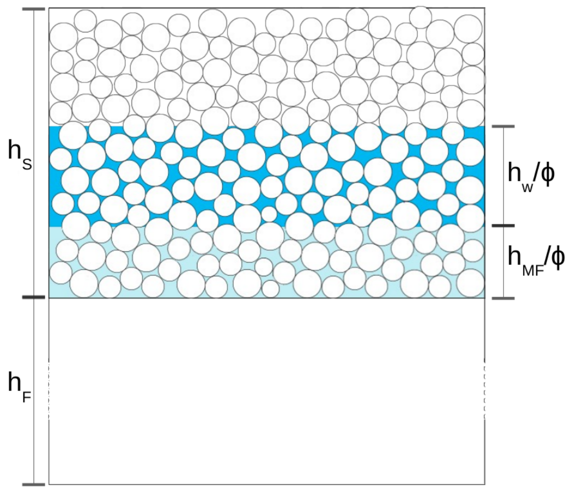

Figure 1. A column of snow and firn.

2.2 Model of snow-firn dynamics

The model is composed of two layers: the snowpack (see Sec. 2.1) and the firn. The firn is modelled as a single impermeable layer of volume V_F with unitary area, height h_F, mass M_F and density ρ_F (Fig. 1). The amount of water percolation inside the firn, neglected in this version of the model, varies greatly depending on the type of glacier. At high altitudes, where maximum temperatures are rarely positive, the effects of percolation due to melting are limited (Smiraglia et al., 2000); at the cold site of Colle Gnifetti, where the model was applied, percolation occurs only in the few centimetres below the surface and it does not involve previous year layers (Alean et al., 1983).

In order to separate snow from firn we refer to its original definition that defines firn as snow that has survived one melt season (Cuffey and Paterson, 2010).

2.2.1 Equations of the model

The model consists of six ODEs: the four equations of the snow model with in addition the mass balance and momentum balance of firn. The mass variation of firn is obtained considering firn melt, the effects of precipitation on firn and the transformation of snow in firn at the end of each water year. The firn densification rate is obtained considering a densification due to overburden stress and a densification due to addition of new mass. Accordingly, the resulting system is as follows (see

https://doi.org/10.5194/tc-2020-357
Preprint. Discussion started: 21 January 2021

Appendix A for the derivation of the system and the detailed description of the terms in the equations):

$$\frac{dh_S}{dt} = -\frac{h_S}{\rho_S}\frac{d\rho_S}{dt} + \frac{\rho_{NS}}{\rho_S}s - (I\cdot a)(T_A - T_\tau) - \frac{Q}{\rho_S} - \sum_i \frac{h_S}{dt}\delta(t-t_i) \tag{2a}$$

$$\frac{dh_W}{dt} = r + \frac{\rho_S}{\rho_W}(I\cdot a)(T_A - T_\tau) + (I^*\cdot e\cdot a)(T_A - T_\tau) - \alpha\cdot K_W - \sum_i \frac{h_W}{dt}\delta(t-t_i) \tag{2b}$$

$$\frac{dh_{MF}}{dt} = -\frac{\rho_W}{\rho_i}(I^*\cdot e\cdot a)(T_A - T_\tau) - \sum_i \frac{h_{MF}}{dt}\delta(t-t_i) \tag{2c}$$

$$\frac{dh_F}{dt} = -\frac{h_F}{\rho_F}\frac{d\rho_F}{dt} - (I_F\cdot a)(T_A - T_\tau)\delta(h_S) + \frac{\rho_W}{\rho_F}r\delta(h_S)\langle T_\tau - T_A\rangle + \sum_i \frac{\rho}{\rho_F}\frac{h}{dt}\delta(t-t_i) \tag{2d}$$

$$\frac{d\rho_S}{dt} = (c\cdot A_1\cdot U)\rho_S\exp(-B\cdot(T_\tau - T_S) - A_2\cdot\rho_S) + \frac{\rho_{NS}-\rho_S}{h_S}s \tag{2e}$$

$$\frac{d\rho_F}{dt} = \frac{d\rho_F}{dt}\Big|_{comp} + \sum_i \frac{\rho-\rho_F}{h_F}\left(\frac{h}{dt}\right)\delta(t-t_i) \tag{2f}$$

The last terms in Eqs. (2a–2c) move, at the end of each melt season, the remaining snowpack (if present) in the firn layer; t_i is the time instant at the end of water year i and $\delta(.)$ is the Dirac delta function equal to 1 when the argument is 0 and 0 otherwise. In Eq. (2d), I_F is the product of a binary function equal to 1 if $T_A \geq T_\tau$ and of a function of h_F, namely $\frac{h_F}{h_F+k}$, which tends to 0 with h_F, with k specified above.

In Eq. (2f), the densification due to compaction ($\frac{d\rho_F}{dt}|_{comp}$) is obtained adopting the model of Arnaud et al. (2000) with some of the modifications proposed by Bréant et al. (2017). Accordingly,

$$\frac{d\rho_F}{dt}\Big|_{comp} = \begin{cases} \gamma\frac{\max(P,10^4\ \mathrm{Pa})}{(\rho_F/\rho_i)^2}\left(1+\frac{0.5}{6}-\frac{5}{3}\frac{\rho_F}{\rho_i}\right)\rho_i & \rho_F/\rho_i \leq D_0 \\ 5.3A\cdot\left((\rho_F/\rho_i)^2 D_0\right)^{1/3}\left(\frac{a_c}{\pi}\right)^{1/2}\left(\frac{4\pi\cdot P\cdot\rho_i}{3a_c\cdot Z\cdot\rho_F}\right)^3\rho_i & D_0 < \rho_F/\rho_i \leq D_c \\ 2A\cdot\frac{\rho_F(1-\rho_F/\rho_i)}{\rho_i(1-(1-\rho_F/\rho_i)^{\frac{1}{3}})^3}\left(\frac{2(P-P_b)}{3}\right)^3\rho_i & D_c < \rho_F/\rho_i \leq 0.95 \\ \frac{9}{4}A\cdot(1-\rho_F/\rho_i)(P-P_b)\rho_i & \rho_F/\rho_i > 0.95 \end{cases} \tag{3}$$

In the first stage, P is the overburden pressure (Pa) and $\gamma = \gamma'\exp\left(-\frac{Q_1}{R_G(T_F+273.15)}\right)$ in which R_G is the gas constant, Q_1 an activation energy equal to $48\cdot 10^3\ \mathrm{J\,mol^{-1}}$, γ' a parameter (estimated in Sec. 4.2) and T_F is the average temperature of firn (°C). In the second stage, $A = A_0\exp\left(-\frac{Q_2}{R_G(T_F+273.15)}\right)$ with $A_0 = 2.84\cdot 10^{-11}\ \mathrm{Pa^{-3}\,h^{-1}}$, a_c is the average contact area, Z is the number of particle contacts (see Appendix A for the expression of a_c and Z), Q_2 is an activation energy and D_0 is the relative density at the transition between the first stage and the second stage. The value of Q_2 was set to $60\cdot 10^3\ \mathrm{J\,mol^{-1}}$, as in the model of Arnaud et al. (2000), since it is the typical activation energy associated with self-diffusion of ice. However, at warmer temperature (i.e. higher than -10 °C) a higher activation energy is required to best fit density profiles with firn densification models (Cuffey and Paterson, 2010; Arthern et al., 2010; Jacka and Jun, 1994). A discussion of the thermal variation of the creep parameter and the impact of the different sintering mechanisms on it can be found in Bréant et al. (2017). Lastly, in the third stage, P_b is the pressure inside the bubbles equal to $P_b = P_c\frac{(\rho_F/\rho_i)(1-D_c)}{D_c\cdot(1-\rho_F/\rho_i)}$ with D_c and P_c the relative density and pressure at the transition between second and third stage.

https://doi.org/10.5194/tc-2020-357
Preprint. Discussion started: 21 January 2021

The Cryosphere Discussions

The model of Arnaud et al. (2000) was chosen because it explicitly represents stress, it models non-steady conditions and it includes a more physical description of densification. Nevertheless, the model can be implemented also with a different firn densification model, given that it represents non steady conditions. In particular, the model of Arnaud et al. (2000), that was developed for polar sites, may not be suitable for temperatures too close to 0 °C. Anyway, the possibility to apply a firn densification model developed for polar sites also to warmer firn of mountain glaciers, possibly with some modifications, is shown in Huss (2013) where the model of Herron and Langway (1980), developed for the Greenland ice sheet, was recalibrated and adapted for temperate/polythermal firn.

2.2.2 Temperature profile

The energetic description of the volume was simplified assuming the constituents in thermal equilibrium and assuming a bilinear profile of temperature through depth. Temperature was assumed to vary linearly from surface temperature T_0 to the mean annual firn temperature (MAFT) at the depth z_M at which seasonal variation of temperature is negligible. At depths higher than z_M, temperature was kept constant and equal to MAFT. In cold glaciers the value of MAFT is close to the mean annual air temperature (MAAT) when melt water percolation is limited (Suter et al., 2001) while in temperate glaciers it is equal to the melting temperature (Cuffey and Paterson, 2010). Surface temperature was fixed equal to T_A if $T_A < 0°\mathrm{C}$ and zero elsewhere. Already Huss (2013) assumed a bilinear profile of temperature in order to study temperate firn densification, fixing z_M to 5 m since it is the typical penetration of winter air temperature.

2.3 Numerical model

The model was solved using the forward Euler finite-difference scheme with a fixed time step, Δt, of one hour. To compute the last terms in Eqs. 1d and 2f, also when h_S and h_F are zero, these terms were calculated, following De Michele et al. (2013), as $\frac{\rho_{NS}(t)-\rho_S}{h_S(t)+s(t)\Delta t}s(t)$ and $\frac{\rho(t)-\rho_F}{h_F(t)+h(t)}\frac{h(t)}{\Delta t}$. The model requires the calibration of the two parameters governing the rate of melting of firn and snow and the refreezing inside the snowpack, namely a and e. If data are available, a different value for a could be calibrated for firn and snow.

3 Study area and data

3.1 Study area

The site of Colle Gnifetti (CG) is part of the summit ranges of the Monte Rosa massif, Swiss/Italian Alps. It is the uppermost part of the accumulation area of Grenzgletscher and it forms a saddle that lies between Signalkuppe (4554 $\mathrm{m\,a.s.l.}$) and Zumsteinspitze (4563 $\mathrm{m\,a.s.l.}$) at an altitude of 4400–4550 $\mathrm{m\,a.s.l.}$ (Lüthi and Funk, 2000) (Fig. 2). The glacier at Colle Gnifetti has a thickness between 60 and 120 m and a MAFT of -14 °C (Wagenbach et al., 2012). The regime is that of a high altitude site, i.e. nearly persistent sub-zero air temperature, a high precipitation total and high wind speed (Suter et al., 2001).

https://doi.org/10.5194/tc-2020-357
Preprint. Discussion started: 21 January 2021

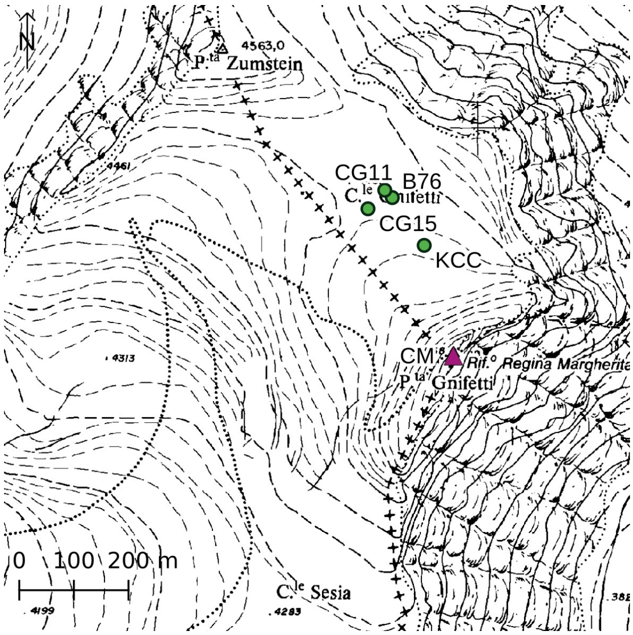

Figure 2. The site of Colle Gnifetti and the location of the ice cores considered in the present work. Source of the basemap: Piedmont Geoportal

A mean annual precipitation of $2.7 \cdot 10^3\ \mathrm{kg\,m^{-2}\,y^{-1}}$ with an interannual variability of $0.8 \cdot 10^3\ \mathrm{kg\,m^{-2}\,y^{-1}}$ (Mariani et al., 2014) was estimated for the period 1961–1993 from a core extracted at upper Grenzgletscher (Eichler et al., 2000).

Even though the site is characterized by high precipitation totals, accumulation in the saddle is considerably lower and highly variable over the glacier surface due to wind erosion, with values ranging from about $0.15 \cdot 10^3\ \mathrm{kg\,m^{-2}\,y^{-1}}$ to $1.2 \cdot 10^3\ \mathrm{kg\,m^{-2}\,y^{-1}}$ depending on the wind exposure (Alean et al., 1983; Lüthi and Funk, 2000; Licciulli et al., 2020). Alean et al. (1983) measured the accumulation at CG between 17 August 1980 and 23 July 1982 with a network of 30 stakes. For the period between 14 August 1981 and 23 July 1982 the mass balance was negative in all the stakes due to wind erosion, while the net accumulation of water year 1980–1981 varied between $+0.04 \cdot 10^3\ \mathrm{kg\,m^{-2}\,y^{-1}}$ and $+1.18 \cdot 10^3\ \mathrm{kg\,m^{-2}\,y^{-1}}$ with the highest values on south facing slopes. This occurs because the enhanced melting and refreezing causes the formation of wet layers and ice crusts and because higher temperatures are associated with a faster densification and both these aspects reduce the possibility of wind to erode snow. This results also in the fact that almost all the snow that survives the melt season comes from summer events (Bohleber et al., 2018; Schöner et al., 2002).

3.2 Data collection

All meteorological data belong to Arpa Piemonte stations (Fig. 3) and they are summarized in Table 1. Information about installed instruments can be found at https://www.arpa.piemonte.it. Hourly data of air temperature and average wind speed at Capanna Regina Margherita (CM) were used as input for the model, daily data at Macugnaga Pecetto (MP) and Macugnaga

https://doi.org/10.5194/tc-2020-357
Preprint. Discussion started: 21 January 2021

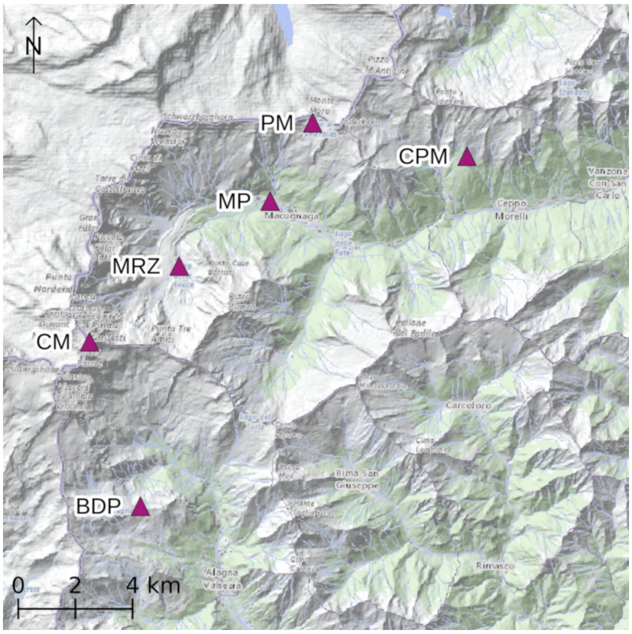

Figure 3. Location of the meteorological stations used: Capanna Regina Margherita (CM), Macugnaga Rifugio Zamboni (MRZ), Macugnaga Pecetto (MP), Ceppo Morelli (CPM), Passo del Moro (PM) and Bocchetta delle Pisse (BDP). Source of the basemap: Arpa Piemonte Geoportal

Rifugio Zamboni (MRZ) were used to reconstruct precipitation series at Colle Gnifetti, hourly data of air temperature along with daily data at Macugnaga Rifugio Zamboni were used to calibrate the parameter a and hourly and daily air temperature data at Macugnaga Pecetto, Passo del Moro (PM), Bocchetta delle Pisse (BDP) and Ceppo Morelli (CPM) were used to infill missing temperature data at Capanna Regina Margherita. In order to compute the snow transport, we considered the average wind speed instead of maximum wind speed, to avoid overestimation due considering a wind speed equal to the maximum one during all the hour.

The station of Capanna Regina Margherita, whose data were used to run the snow-firn model, was installed in 2002 by the Piedmont Region at the Regina Margherita Hut as part of a project that aimed to study the interaction between synoptic flow and orography. With its 4560 m of altitude it can be considered the highest meteorological station in Europe and its wind speed series can be considered representative of the synoptic conditions (Martorina et al., 2003). Due to its recent installation, the use of these data limits the length of the simulation and the number of cores with which our results can be compared. Nevertheless, we believe that, given the peculiar characteristics of the station, the use of these data may give added value to this study.

In Table 2 ice core data are reported (Fig. 2). KCC, CG11 and CG15 were used to validate the model and B76 was used as a reference steady-state depth-density profile while computing the value of parameter γ'.

https://doi.org/10.5194/tc-2020-357
Preprint. Discussion started: 21 January 2021

Table 1. Meteorological data employed in the case study (p stands for precipitation, SD for snow depth, T_A air temperature, u average wind speed and s fresh snow). All stations belong to Arpa Piemonte network. Water years are identified by the first year, e.g. 2008 is water year 2008–2009.

Station name	Altitude (m a.s.l)	UTM X WGS84 (m)	UTM Y WGS84 (m)	Variable	Aggregation	Period used
Macugnaga Pecetto (MP)	1360	419251	5091486	p, SD, T_A, s	Daily	1 October 2002–30 September 2019
Macugnaga Rifugio Zamboni (MRZ)	2075	416068	5089214	p, SD, T_A, s	Daily	1 October 2007–30 September 2019
Macugnaga Rifugio Zamboni (MRZ)	2075	416068	5089214	T_A	Hourly	Water year: 2008, 2009, 2011, 2014 , 2016, 2017
Capanna Regina Margherita (CM)	4560	412930	5086564	T_A, u	Hourly	1 October 2002–13 August 2013
Passo del Moro (PM)	2820	420739	5094227	T_A	Daily	1 October 2002–30 September 2007
Passo del Moro (PM)	2820	420739	5094227	T_A	Hourly	November 2002, September 2007
Bocchetta delle Pisse (BDP)	2410	414709	5080807	T_A	Daily	1 October 2002–30 September 2007
Bocchetta delle Pisse (BDP)	2410	414709	5080807	T_A	Hourly	November 2002, September 2007
Ceppo Morelli (CPM)	1995	426141	5093057	T_A	Daily	1 October 2002–30 September 2007
Ceppo Morelli (CPM)	1995	426141	5093057	T_A	Hourly	November 2002, September 2007

3.3 Data handling

The model requires in input a continuous series of air temperature, precipitation and wind speed.

Following the comparison presented by Henn et al. (2013), to fill missing hourly temperature data at Capanna Margherita, MicroMet procedure (Liston and Elder, 2006) was adopted for gap smaller than 24 hours and a long-term lapse rate approach with five stations (CM, MP, CPM, PM, BDP) was adopted for longer gaps. In the period 1 October 2002–13 August 2013, 0.37 % of hourly temperature data were missing. After MicroMet procedure 0.23 % remained missing and were substituted with a long-term lapse rate approach.

Table 2. Ice core data employed in the case study.

Name	Drilling date	Mean annual accumulation ($10^3\ \mathrm{kg\,m^{-2}\,y^{-1}}$)	Data source
B76	1976	0.37	Gäggeler et al. (1983)
CG15	2015	0.45	Sigl et al. (2018)
CG11	2011	0.41	Ardenghi (2012)
KCC	2013	0.22	Licciulli et al. (2020)

To fill missing wind speed data, MicroMet procedure was used for gaps smaller than 24 hours. For gaps longer than 24 hours, the missing period was substituted with the corresponding measurement of another year. The year was chosen computing the frequency duration curve of wind speed for each year and selecting a year whose behaviour was similar to the average one. In the period 1 October 2002–13 August 2013, 1.3 % of data were missing, that reduced to 1.17 % after MicroMet procedure. Longer gaps were present in three years, namely 2002, 2007 and 2012. The sensitivity of the year chosen was tested computing the net accumulation for the three water years; the largest difference was obtained for water year 2011–2012 that showed a variability between $0.44 \cdot 10^3$ and $0.50 \cdot 10^3\ \mathrm{kg\,m^{-2}\,y^{-1}}$.

Precipitation at CG was reconstructed starting from the corrected daily precipitation series at MP and MRZ. The corrected precipitation series at the two stations was obtained combining the information coming from precipitation series (measured by rain gauges) and fresh snow series (an estimation of snow fallen in the 24 hours before 8 AM of each day obtained from snow depth data). Precipitation data are provided both as the total precipitation fallen in the day and as the total precipitation fallen in the 24 hours before 9 AM; to better compare precipitation with fresh snow data, the latter was chosen. To obtain total precipitation, firstly the processed series of fresh snow in water equivalent, called s_w, was obtained as follows: (1) missing data of fresh snow in days with average daily air temperature greater than 0 °C were set to zero (fresh snow reported at 8 AM was associated with the previous day temperature); (2) all other missing data were estimated from the difference between the previous and next non missing snow depth data; (3) fresh snow was transformed in water equivalent computing fresh snow density following Anderson (1976). Secondly, total and liquid precipitation series, called p and p_r respectively, were reconstructed as follows: (1) missing data of precipitation during days with average air temperature lower than 0 °C were set to zero; (2) a first estimation of rain was obtained setting p_r equal to $p - s_w$ if the difference was positive and zero otherwise and setting it missing if p or s_w were missing; (3) total precipitation p was recomputed summing p_r and s_w; (4) every missing value of p in one station corresponding to a non missing value in the other one was substituted estimating an average increase of precipitation with altitude:

$$m_p = \frac{1}{n} \sum_{i=1}^{n} \frac{p_{i,MP} - p_{i,MRZ}}{z_{i,MP} - z_{i,MRZ}} \tag{4}$$

https://doi.org/10.5194/tc-2020-357
Preprint. Discussion started: 21 January 2021

where z is the altitude and m_p was calculated considering only days with precipitation; (5) precipitation data still missing after these steps were set to zero; (6) rain was recomputed as in step 3.

In order to extrapolate precipitation at the altitude of CG, it is necessary to take into account that precipitation does not increase indefinitely with altitude but at one point along the slope it reaches a maximum, after which it starts decreasing. The altitude of maximum precipitation is the result of two opposite phenomena that are at the base of orographic precipitation: the enhanced moisture condensation due to air lifting and the exponential decrease in the amount of available moisture with height following Clausius–Clapeyron (Roe, 2005). We therefore decided to assume a linear increase of precipitation up to an altitude z_m and then to keep precipitation constant. Since studies about the altitude of maximum precipitation for the Monte Rosa massif were not found, the formula proposed by Alpert (1986) for a bell shaped mountain was adopted. The formula is derived from the continuity equation of water vapour and it links z_m to the mountain height H and the temperature lapse rate Γ as follows:

$$z_m = \frac{3H}{(4 - 0.12 \cdot \Gamma H + 0.0036 \cdot \Gamma^2 H^2)^{1/2} + 0.06 \cdot \Gamma H + 2} \tag{5}$$

In this case, $H = 4634$ m and $\Gamma = 0.0058\ °\mathrm{C\,m^{-1}}$ using the average value between CM and MP.

Given z_m and m_p (from Eq.4), precipitation at CG can be estimated for each day i from the series p of MP as follows: $p_{i,CM} = p_{i,MP} + m_p(z_m - z_{MP})$ if $p_{i,MP} > 0\ \mathrm{mm\,d^{-1}}$ and $p_{i,CM} = 0\ \mathrm{mm\,d^{-1}}$ otherwise. Precipitation was then divided equally over the 24 hours and a threshold of 1 °C was chosen to distinguish between solid and liquid precipitation, since this is the value generally found in Europe (Jennings et al., 2018).

3.4 Model's parameters

The parameter e requires data of snow density or snow water equivalent to be calibrated. Since they were not available, its value was set to 0.2, that is the median value obtained by Avanzi et al. (2015) for a Japanese site. The parameter a was calibrated running the snow model without the wind contribution at MRZ with an hourly time step. For each water year in Table 1 (i.e. 2008-2009, 2009-2010, 2011-2012, 2014-2015, 2016-2017 and 2017-2018) we estimated the parameter using least squares on daily snow depth data and minimizing the objective function with a population-evolution-based algorithm, namely SCE-UA (Shuffled Complex Evolution-University of Arizona) (Duan et al., 1992, 1993). To evaluate the model, for each calibrated parameter, we computed the NSE (Nash-Sutcliffe Efficiency) between observed and modelled snow depth for all water years except the one used to calibrate the parameter. The median value of a was selected and used in the snow-firn model. The parameter γ', that governs firn densification rate, was estimated running the firn densification model in a steady-state condition (Bader, 1954), setting $T_F = -14.1$ °C (Haeberli and Funk, 1991), the mean accumulation rate and surface density to the one of B76 ice core (see Table 2), $D_0 = 0.56$ (Bréant et al., 2017), $P_c = 740 \cdot 10^2$ Pa (Lüthi and Funk, 2000) and $D_c = 0.85$ since the precise value is not known at CG (Lüthi and Funk, 2000). The other parameters of the snow-firn model that require to be specified are z_M and MAFT set to 5 m and -14.1 °C (Haeberli and Funk, 1991) and the grain radius R that influences the threshold wind speed. It is defined as $R = 3/(\rho_i SSA)$ where SSA is the specific surface area in $\mathrm{m^2\,kg^{-1}}$. SSA was computed adopting the parametrization of Domine et al. (2007) for recent snow, $SSA = -16.051 \ln(\rho_S \cdot 10^{-3}) + 7.01$.

https://doi.org/10.5194/tc-2020-357
Preprint. Discussion started: 21 January 2021

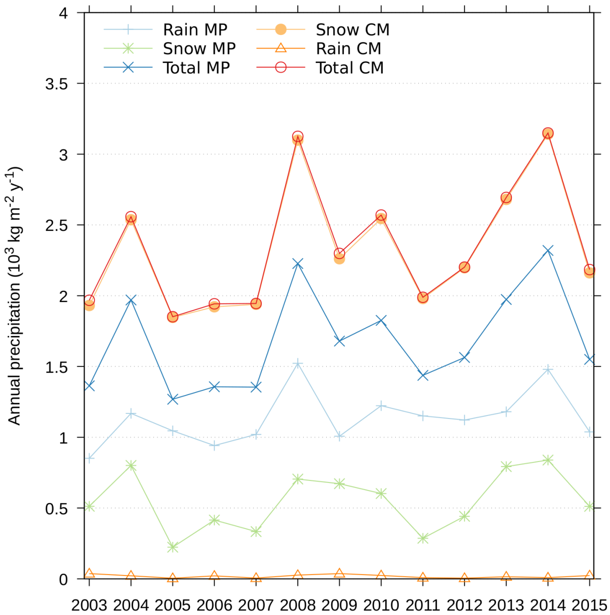

Figure 4. Annual precipitation at Macugnaga Pecetto (MP), obtained from the processed precipitation series, and at Capanna Margherita (CM), obtained from the reconstructed precipitation series.

4 Results

4.1 Reconstructed precipitation at CM

From Eqs. (4, 5) we obtained $m_p = 0.004\ \mathrm{mm\,d^{-1}\,m^{-1}}$ and $z_m = 2547\ \mathrm{m}$. The altitude of maximum precipitation was found away from the crest as it is typical for large mountains (Roe, 2005). The reconstructed annual totals are reported in Fig. 4 subdivided in liquid and solid events. The average for the period 2003–2015 is $2.35 \cdot 10^3\ \mathrm{kg\,m^{-2}\,y^{-1}}$ that can be confronted with the average for the period 1961–1993 of $2.7 \cdot 10^3\ \mathrm{kg\,m^{-2}\,y^{-1}}$ estimated from the upper Grenzgletscher core (see Section 3.1). An average annual precipitation of $3.5 \cdot 10^3\ \mathrm{kg\,m^{-2}\,y^{-1}}$ and $1.7 \cdot 10^3\ \mathrm{kg\,m^{-2}\,y^{-1}}$ would have been estimated using, respectively, the altitude of Capanna Margherita as z_m and the processed series of Macugnaga Pecetto not increased with altitude.

4.2 Parameters' estimation

We obtained a median value of the parameter a of $3.84 \cdot 10^{-4}\ \mathrm{m\,h^{-1}\,{}^\circ C^{-1}}$ with an average NSE of 0.71 in validation. The value is in the range obtained by Avanzi et al. (2014) for a selection of forty sites within the SNOTEL network. The estimated value of the parameter γ' is 1.26 $\mathrm{Pa^{-1}\,h^{-1}}$ with the resulting profile reported in Fig. 5.

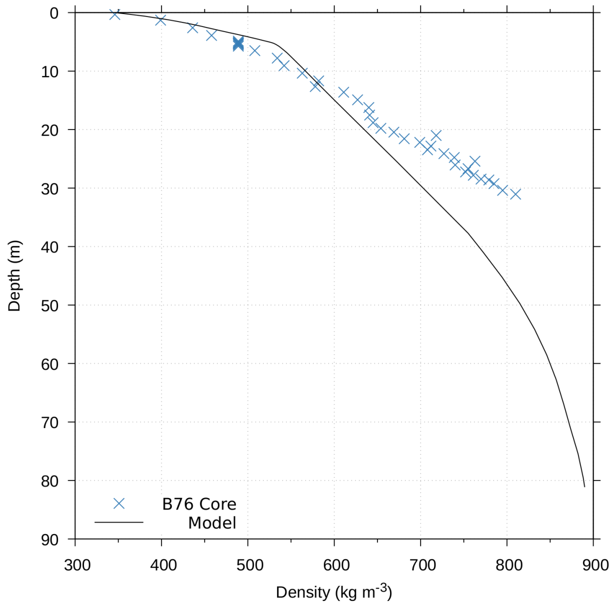

Figure 5. Firn densification model for steady-state conditions and density profile of B76 ice core.

Table 3. Modelled and observed mean (μ) and standard deviation (σ) of the accumulation rate for the period 2003–2012.

	μ (10^3 kg m^{-2} y^{-1})	σ (10^3 kg m^{-2} y^{-1})
Model	0.26	0.10
CG11	0.41	0.09
KCC	0.30	0.09
CG15	0.36	0.15

4.3 Snow accumulation

The annual accumulation obtained from the snow-firn model is reported in Fig. 6 along with the values retrieved from the three available ice cores, the average value of the observations and its 95% confidence interval. The Root Mean Square Error (RMSE) between the model and the average of the observations is equal to $0.17 \cdot 10^3$ kg m^{-2} y^{-1}, while the modelled and observed average annual accumulation and standard deviation are reported in Table 3.

In order to better understand the characteristics of the accumulation at CG the monthly box plot of solid precipitation, snow transport, monthly contribution to annual accumulation and number of hours with $T_A > 0$ °C, that in the model correspond to hours with melting, are provided in Figs. 7–10. Since snow is moved into firn at the end of September and wind is not allowed to erode firn, the fraction of conserved snow of September may be overestimated and the snow transport of October

https://doi.org/10.5194/tc-2020-357
Preprint. Discussion started: 21 January 2021

The Cryosphere Discussions

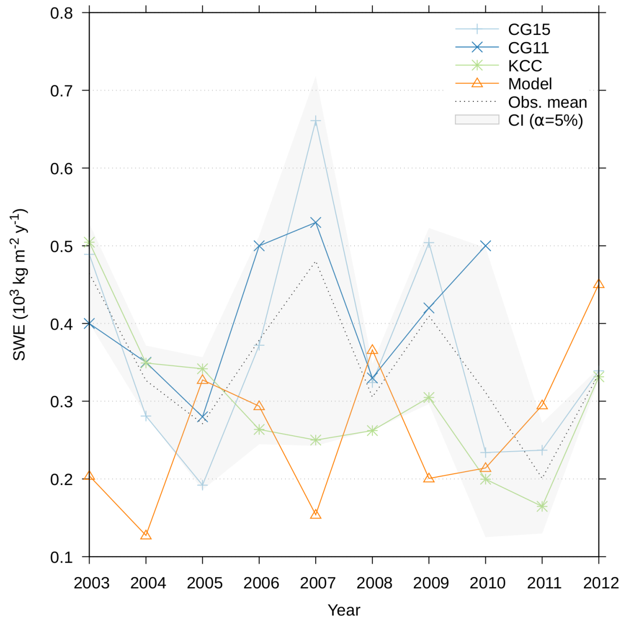

Figure 6. Annual accumulation modelled and retrieved from three ice cores. The average of the annual accumulations from ice cores and its 95% confidence interval are also reported.

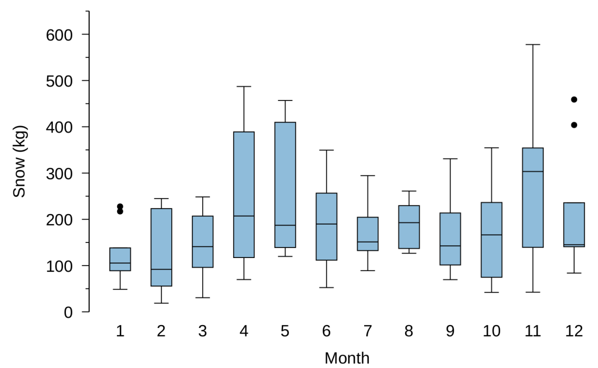

Figure 7. Box plot of monthly solid precipitation.

underestimated. We can see that annual accumulation is composed by snow deposited mainly between May and September, with July the month that in average contributes the most. The months in which solid precipitation is conserved are also the months in which temperature goes above the melting point; winter snow, instead, is completely removed.

https://doi.org/10.5194/tc-2020-357
Preprint. Discussion started: 21 January 2021

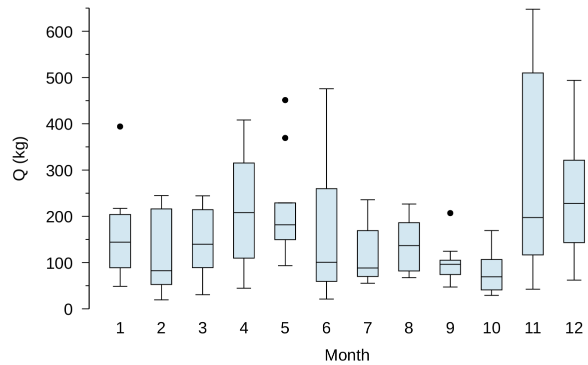

Figure 8. Box plot of monthly snow transport.

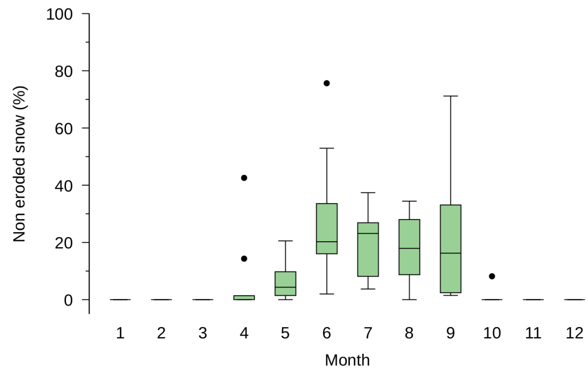

Figure 9. Box plot of monthly fraction of conserved solid precipitation.

310 ## 4.4 Firn density

The modelled firn density was confronted with the density estimated from KCC core (Fig. 11). Since the model returns the average density of all the firn column and not the density of each annual layer, to confront them the model was run for an increasing number of years and the corresponding observed density was obtained averaging the density of the layers deposited in the same range of years. The model was always run up to 13 August 2013, the KCC drilling date, in order to reproduce
315 the same conditions experienced by the ice core. The RMSE is 8.16 $\mathrm{kg\,m^{-3}}$ with a maximum difference of about 20 $\mathrm{kg\,m^{-3}}$ corresponding to the average density of the layer deposited in 2012.

https://doi.org/10.5194/tc-2020-357
Preprint. Discussion started: 21 January 2021

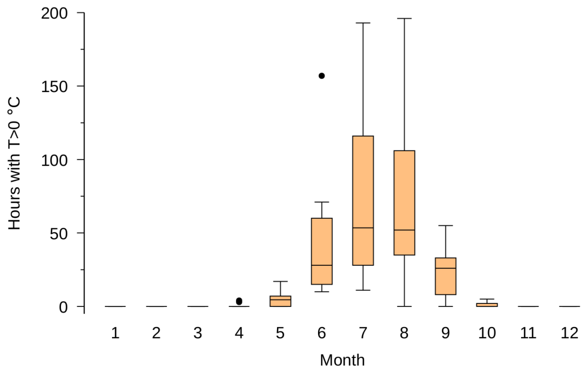

Figure 10. Box plot of monthly number of hours with above zero temperatures.

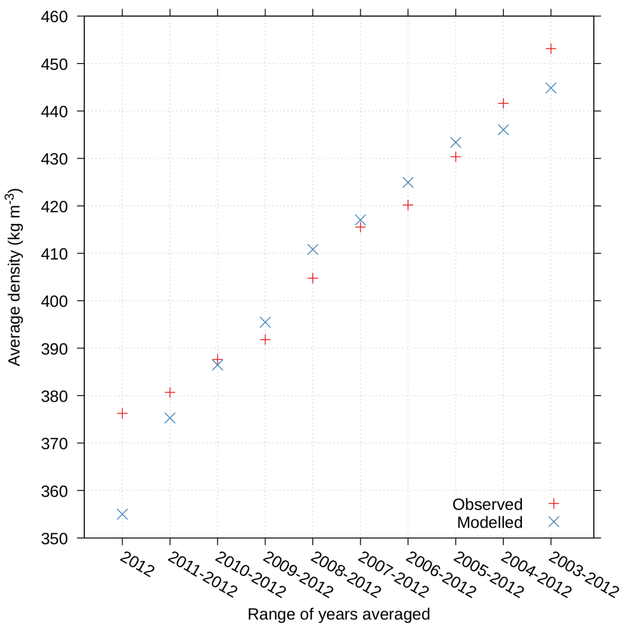

Figure 11. Observed and modelled average firn density. The range of years in the x-axis indicates the deposition year of the layers whose density was averaged. The firn densities, modelled and observed, are referred to August 2013.

5 Discussion

5.1 Snow accumulation

Snow accumulation at CG is characterized by a high spatial variability (Keck, 2001; Licciulli et al., 2020). The difference
320 in net annual accumulation of CG11 and CG15, that are about 50 m apart, ranges from $+0.13 \cdot 10^3\ \mathrm{kg\,m^{-2}\,y^{-1}}$ to $-0.266 \cdot 10^3\ \mathrm{kg\,m^{-2}\,y^{-1}}$ in the period 2002–2012, while the one of CG15 and KCC, that are about 120 m apart, ranges between

$+0.41 \cdot 10^3\ \mathrm{kg\,m^{-2}\,y^{-1}}$ and $-0.15 \cdot 10^3\ \mathrm{kg\,m^{-2}\,y^{-1}}$. The accumulation is strongly affected by surface topography that in turn is influenced by wind; this results in a quasi random spatial variation and a systematic temporal variation at a given location (Keck, 2001). Given the high variability in the accumulation rate, three ice cores may not be enough to fully represent the site, besides, ice core data are biased due to the fact they are drilled preferentially in the north flank, where accumulation and radiation are lower. While the modelled average annual accumulation is in the range of the ones estimated for the north flank of CG (Licciulli et al., 2020), the model is not able to reproduce the observed spatial variability. This would require to consider the effect of topography on wind speed and the spatial variation in solar radiation. Surface snow temperature was set equal to air temperature, instead of solving the full surface energy balance that would have required a higher availability of data; surface temperatures, in fact, may reach $0\ ^\circ\mathrm{C}$ also for air temperatures below $0\ ^\circ\mathrm{C}$ mainly when calm conditions are present or, on the contrary, melting may not occur during positive air temperatures particularly when wind is present (Keck, 2001).

In accordance with the box plot in Figs. 7–10, different works that studied ice cores drilled at CG report that snow accumulation is mainly made up by precipitation of the warm seasons (Wagenbach et al., 1988; Schöner et al., 2002; Bohleber et al., 2013, 2018). Also at Seserjoch (Colle Sesia in Fig. 2), 4300 m a.s.l., where snow height was measured between 1998 and 2000 by Suter et al. (2001), a main accumulation from about April to November, with practically no accumulation in high winter was observed. Figure 9 shows that the conserved fraction of solid precipitation reflects the number of hours with greater than zero temperature rather than the seasonality of precipitation. Accumulation is, in fact, mainly governed by wind erosion (Wagenbach et al., 1988) and the presence of wet layers or ice crusts as well as a faster compaction when temperatures are higher protect snow from wind erosion. This could lead, as already suggested by Alean et al. (1983), to a counterintuitive response in a scenario of greater temperatures, since the increased melting and the reduced fraction of solid events with respect to total precipitation will be accompanied by a reduced snow erosion. An increase of positive net balances may in turn influence ice avalanche activity. Future applications of the model may address the answer of the site in term of snow accumulation under scenarios of climate warming.

5.2 Firn density

The observed and modelled densities show a good agreement up to the densities reached by the model, even though to validate the ability of the model to reproduce firn densification up to glacier ice, a longer series of meteorological data is needed. The absence of snow density or water equivalent measures doesn't allow to validate the modelled surface snow density, whose underestimation may be the reason of the difference between observed and modelled density of 2012 firn layer. Surface density at CG is, in fact, difficult to measure and highly variable since it depends on aspect and wind exposure (Licciulli et al., 2020). Wind speed, in fact, affects snow and firn densification as well as snow accumulation when snow drift occurs (Keenan et al., 2020). Its influence was tested running the model neglecting wind contribution U in Eq. 1d, i.e. fixing its value to $1\ \mathrm{m\,s^{-1}}$, and extracting the same data of Fig. 11. An increase of RMSE from $8.16\ \mathrm{kg\,m^{-3}}$ to $12.35\ \mathrm{kg\,m^{-3}}$ was obtained with a systematic underestimation of average firn density.

https://doi.org/10.5194/tc-2020-357
Preprint. Discussion started: 21 January 2021

6 Conclusions

In this study we have proposed a local model that combines snow and firn dynamics. It consists of six ODEs derived from the mass balance, momentum balance and rheological equations of snow and firn. The model has a parsimonious parametrization, with three parameters (a, e, γ') to be estimated. The model requires in input a series of hourly (or sub-hourly) series of precipitation, temperature and wind speed with which the series of snow, water and ice inside the snowpack and firn height along with dry snow and firn density are computed. The model was applied to the site of Colle Gnifetti (Monte Rosa massif, 4400–4550 $\mathrm{m\,a.s.l.}$) for a period of 10 years. The application of the model to a high altitude site allowed us to explore two main problems: the low availability of measured data and the strong influence of wind on snow accumulation and densification. The modelled average net accumulation is equal to $0.26 \cdot 10^3\ \mathrm{kg\,m^{-2}\,y^{-1}}$ against an average precipitation above $2 \cdot 10^3\ \mathrm{kg\,m^{-2}\,y^{-1}}$, with a monthly distribution of the conserved snow that reflects the number of melting events rather than the precipitation seasonality, as observed also from ice cores. The model is not able to reproduce the strong spatial variability of snow accumulation, that would probably require to take in consideration the influence of topography on wind speed and the spatial variation of solar radiation. The modelled density profile shows a good agreement with observed data, even though a longer time series is required to confirm this result for densities up to glacier ice density. The application of the model to other sites with a greater availability of data as well as a sensitivity analysis of the chosen parameters will be carried out for a more robust validation of the model along with the possibility to include it inside a distributed hydrological model.

Appendix A: Complete description and derivation of the snow-firn model

A1 Mass balance equations

The mass balance equations of snow (M_S), liquid water in snow (M_W), iced water in snow (M_{MF}), and firn (M_F) are as follows:

$$\frac{dM_S}{dt} = P_S - M - Q - E_S \tag{A1a}$$

$$\frac{dM_W}{dt} = P_R + M + F - O - E_W \tag{A1b}$$

$$\frac{dM_{MF}}{dt} = -F - E_{MF} \tag{A1c}$$

$$\frac{dM_F}{dt} = -O_F + P_F + E_S + E_W + E_{MF} \tag{A1d}$$

P_S and P_R are the mass of solid and liquid precipitation events and they are equal to $P_S = s \cdot \rho_{NS}$ and $P_R = r \cdot \rho_W$. Following Anderson (1976), $\rho_{NS} = 50\,\mathrm{kg\,m^{-3}}$ if the air temperature $T_A < -15°C$ and $\rho_{NS} = 50 + 1.7 \cdot (T_A + 15)^{1.5}\ \mathrm{kg\,m^{-3}}$ otherwise.

M is the snow melt mass flux that was computed with a temperature-index approach (Hock, 2003). Accordingly, $M = (I \cdot a)(T_A - T_\tau)\rho_S$.

F is the melt freeze mass flux that was modelled with a coupled melt-freeze temperature-index approach. Accordingly, $F = (I^* \cdot e \cdot a)(T_A - T_\tau)\rho_W$.

https://doi.org/10.5194/tc-2020-357
Preprint. Discussion started: 21 January 2021

The run-off O was modelled with a matrix flow approach and it is equal to $O = \rho_W \alpha K_W$ where $\alpha = \alpha'(5.47 \cdot 10^5\ \mathrm{m^{-1}\,s^{-1}})$ (DeWalle and Rango, 2008) with α' a time conversion constant equal to $3600\ \mathrm{s\,h^{-1}}$. Following Colbeck (1972), K_W was computed as $K_W = KS^{*3}$ in which K is the intrinsic permeability of snow in $\mathrm{m^2}$ and S^* is the effective saturation degree of the mixture equal to $S^* = (S_r - S_{r_i})/(1 - S_{r_i})$ where S_{r_i} is the irreducible saturation degree equal to $S_{r_i} = 0.02\rho_S/(\rho_W \phi)$ (Kelleners et al., 2009) and S_r is the average saturation degree of the porous matrix equal to 1 when $h_W \geq \phi h_S$ while $S_r = h_W/(\phi h_S)$ otherwise (Avanzi et al., 2015). The intrinsic permeability is calculated using the parametrization proposed by Calonne et al. (2012) and it is equal to $K = 3R^2 \exp(-0.013\rho_S)$ in which R is the equivalent sphere radius defined as $R = 3/(SSA\rho_i)$ where SSA is the specific surface area in $\mathrm{m^2\,kg^{-1}}$ that was computed by Avanzi et al. (2015) adapting the formula proposed by Domine et al. (2007). Accordingly, $SSA = -30.82\ln(\rho_S \cdot 10^{-3}) - 20.60$. When $S_r > 0.5$, to avoid numerical instability, the run-off was calculated with a kinematic wave approximation (De Michele et al., 2013) as $\rho_W \theta_W h_W^{1.25}$.

The firn melting O_F, that may occur only when the snowpack is absent, was modelled with a temperature-index approach and it is equal to $O_F = (I_F \cdot a)(T_A - T_\tau)\rho_F \delta(h_S)$.

P_F is the effect of rain on firn that, when the snowpack is absent, causes an increase of M_F when $T_A < 0\,°\mathrm{C}$ because rainfall is chilled to the firn temperature and a decrease when $T_A > 0\,°\mathrm{C}$ because the energy supplied by rain will be used to melt ice. In the first case $P_F = \rho_W \cdot r$ while in the second case P_F was set to zero due to its small contribution to mass balance (Doyle et al., 2015).

The terms E_S, E_W, E_{MF} move the mass of the snowpack still on the ground at the end of each melt season inside the firn and they are equal to $E_j = \sum_i \rho_j \frac{h_j}{dt}\delta(t - t_i)$ with $j = S, MF, W$.

Q is the mass of snow eroded by wind obtained from snow transport. The latter was computed adopting the parametrization proposed by Pomeroy et al. (1993) as the sum of a transport in saltation and a transport in suspension.

The saltation transport rate Q_{salt} ($\mathrm{kg\,m^{-1}\,s^{-1}}$) occurs only when wind exceeds a given threshold and it is computed as follows:

$$Q_{salt} = \frac{0.68\rho_a u_t^*}{u^* g}(u^{*^2} - u_t^{*^2}) \tag{A2}$$

where ρ_a is the atmospheric density ($\mathrm{kg\,m^{-3}}$) and u^* and u_t^* are respectively the atmospheric friction velocity and the friction velocity applied to the snow surface at the transport threshold ($\mathrm{m\,s^{-1}}$). To move from the measured wind speed u to u^*, knowledge of the aerodynamic roughness height z_0 is required. This passage is not straightforward since the value of z_0 during blowing snow events is different from the one during non transport conditions and it depends on friction velocity (Pomeroy and Gray, 1990). In order to avoid an iterative procedure, we adopted the approximation proposed by Pomeroy and Gray (1990). Accordingly, $u^* \approx 0.02264u^{1.295}$ and $z_0 = \frac{0.1203u^{*^2}}{2g}$ where u is 10 m wind speed ($\mathrm{m\,s^{-1}}$).

Suspension transport, that occurs only when particles are already in saltation, was computed as follows:

$$Q_{susp} = \frac{u^*}{\kappa}\int_{h^*}^{z_b} \eta(z)\ln\left(\frac{z}{z_0}\right)dz \tag{A3}$$

where Q_{susp} is in $\mathrm{kg\,m^{-1}\,s^{-1}}$, κ is the von Kármán constant equal to 0.4, h^* is the lower boundary for suspension equal to $h^* = c_H u^{*^{1.27}}$ (Pomeroy and Male, 1992) with $c_H = 0.08436\ \mathrm{m^{-0.27}\,s^{1.27}}$, z_b is the top of the surface boundary-layer for

https://doi.org/10.5194/tc-2020-357
Preprint. Discussion started: 21 January 2021

suspended snow and $\eta(z)$ is the mass concentration of suspended snow ($\mathrm{kg\,m^{-3}}$) at height z. The mass concentration can be approximate as $\eta(z) = \eta(z_r)\exp(-A_Q((B_Q u^*)^{-0.544} - z^{-0.544}))$ (Pomeroy and Male, 1992) where $\eta(z_r)$ is the reference mass concentration for suspension set to 0.8 $\mathrm{kg\,m^{-3}}$ (Pomeroy and Male, 1992), A_Q is equal to 1.55 $\mathrm{m}^{0.544}$ and B_Q to 0.05628 $\mathrm{s}^{-0.544}$. z_b was set to 5 m, since its value is typically between 5 m and 10 m (Déry and Taylor, 1996). The exact value is unimportant because of small mass fluxes at this height (Pomeroy et al., 1993). The snow erosion in the control volume of the model was set equal to the sum of these two transports.

The critical threshold, above which snow transport occurs, was computed adopting the formula proposed by He and Ohara (2017). Accordingly, the critical shear stress for snow movement can be computed as:

$$\tau_t = \frac{(8R \cdot C_g \cdot g)(\rho_S - \rho_a)\cos(\pi/3 - S) + (\pi C_c \varsigma)\left(\frac{C}{R^m} t_d\right)^{2/n}\left(\sin(\pi/3 + S) + \left(\frac{C}{R^m} t_d\right)^{1/n}\right)}{2\left(C_d \sin(\pi/3 - S) + C_l \cos(\pi/3 - S)\right)} \tag{A4}$$

where R is the grain radius (m), t_d is the time since deposition in seconds, C_c, C_d, C_g and C_l are dimensionless coefficients set to 1, 4, $1.3\pi/6$ and 3.4 (He and Ohara, 2017), ς is the stress caused by cohesion of ice computed as $\varsigma = 1.51\exp(0.44(T_A + 9)) + 6.8$ (Hosler et al., 1957) for temperatures between -20 °C and 0 °C with ς in $\mathrm{N\,m^{-2}}$ and T_A in °C and $S = \arcsin\left(\left(\frac{C}{R^m} t_d\right)^{1/n}\right)$. C, m and n are parameters that influence the rate of ice sintering, modelled following Maeno and Arakawa (2004). Accordingly, $C = C_0 \exp\left(\frac{-Q_s}{R_G(T_A + 273.15)}\right)$ in which R_G is the gas constant and T_A is computed as the average air temperature since deposition, $C_0 = 4.14 \cdot 10^{19}\ \mathrm{m^3\,s^{-1}}$ and $Q_s = 1.965 \cdot 10^5\ \mathrm{J\,mol^{-1}}$. Finally, m and n are empirical parameters set to 2.9 and 5 respectively following the results of He and Ohara (2017). Once the critical shear stress is obtained it is possible to move to critical friction velocity as follows: $u_t^* = \sqrt{\tau_t/\rho_a}$.

Given that $M_j = \rho_j h_j$ and $\rho_k = \mathrm{const}$ with $j = S, MF, W$ and $k = MF, W$, after some algebra we can move from Eqs. A1a–A1d to Eqs. 2a–2d

A2 Snow and firn densification

The densification of dry snow due to compaction was modelled adopting the formula proposed by Liston et al. (2007). Accordingly,

$$\frac{d\rho_S}{dt} = (c \cdot A_1 \cdot U)\rho_S \exp(-B \cdot (T_\tau - T_S) - A_2 \cdot \rho_S) \tag{A5}$$

where $c = 0.10 \cdot 3600\ \mathrm{s\,h^{-1}}$, $A_1 = 0.0013\ \mathrm{m^{-1}}$, $A_2 = 0.021\ \mathrm{m^3\,kg^{-1}}$, $B = 0.08\ \mathrm{K^{-1}}$ and U is the wind speed contribution ($\mathrm{m\,s^{-1}}$). For wind speeds $\geq 5\ \mathrm{m\,s^{-1}}$, $U = E_1 + E_2(1.0 - \exp(-E_3(u_2 - 5.0)))$ with E_1, E_2 and E_3 equal to 5.0 $\mathrm{m\,s^{-1}}$, 15.0 $\mathrm{m\,s^{-1}}$ and 0.2 $\mathrm{m\,s^{-1}}$, respectively, and u_2 the wind speed at 2 m height. For wind speed $< 5\ \mathrm{m\,s^{-1}}$, $U = 1\ \mathrm{m\,s^{-1}}$ Adding the densification due to mass variation (see De Michele et al. (2013)) the total densification rate can be computed as follows:

$$\frac{d\rho_S}{dt} = (c \cdot A_1 \cdot U)\rho_S \exp(-B \cdot (T_\tau - T_S) - A_2 \cdot \rho_S) + \frac{\rho_{NS} - \rho_S}{h_S} s \tag{A6}$$

where we assumed that melting events and snow erosion occur at $\rho_S = \mathrm{const}$.

The densification of firn due to compaction is obtained adopting the model of Arnaud et al. (2000) with some of the modifications proposed by Bréant et al. (2017). The model separates the densification of firn into three stages. The first stage is

https://doi.org/10.5194/tc-2020-357
Preprint. Discussion started: 21 January 2021

governed by settling and it is modelled by Bréant et al. (2017) adapting the equation proposed by Alley (1987). The second stage, that starts when the relative density $D = \rho_F/\rho_i$ equals D_0, is dominated by power law creep and it is modelled following Arzt (1982) and Arzt et al. (1983). Grains are considered as spheres and each sphere is allowed to increase in radius around fixed centres. Starting form an initial radius l, the new radius l' (in units of the initial particle radius l) is $l'(D) = (D/D_0)^{1/3}$. The growth of spheres increases the number of particle contacts Z from the initial value Z_0 to $Z(D) = Z_0 + b(l' - 1)$ in which $b = 15.5$. The overlap due to the growth of particles produces an excess volume of material. This excess is distributed uniformly around the portion of the surface of the spheres not in contact. From this excess volume, it is possible to calculate the new radius l'' as

$$l'' = l' + \frac{4Z_0(l'-1)^2(2l'+1) + b(l'-1)^3(3l'+1)}{12l'\left(4l' - 2Z_0(l'-1) - b(l'-1)^2\right)} \tag{A7}$$

The average contact area (in unit of l^2) can be obtained averaging over all of existing contacts:

$$a(D) = a(l'') = \frac{\pi}{3Zl'^2}\left(3(l''^2 - 1)Z_0 + l''^2 b(2l'' - 3) + b\right) \tag{A8}$$

The value of Z_0 for a given value of D_0 is obtained, as proposed by Arnaud et al. (2000), assuming that the effective stress $P^* = (4\pi P)/(a_c Z D)$ approaches P as D tends to 1. The third stage begins when pores start becoming isolated ($D > D_c$) and densification is calculated considering the deformation of ice shells surrounding cylindrical pores (Wilkinson and Ashby, 1975). As for Eq. 2e, the total densification rate is obtained adding the densification due to new mass addition (Eq. 2f).

Appendix B: List of all the symbols used

https://doi.org/10.5194/tc-2020-357
Preprint. Discussion started: 21 January 2021

The Cryosphere Discussions
Open Access
EGU

Table B1. List of the symbols used (from A to I)

Symbol	Description	Type	Unit
A	creep constant function of T_F	constant	$\mathrm{Pa^{-3}\,h^{-1}}$
A_0	constant governing firn densification	constant	$\mathrm{Pa^{-3}\,h^{-1}}$
A_1	constant governing snow densification	constant	$\mathrm{m^{-1}}$
A_2	constant governing snow densification	constant	$\mathrm{m^3\,kg^{-1}}$
A_Q	constant governing the mass concentration of suspended snow	constant	$\mathrm{m^{0.544}}$
a	degree hour parameter	**calibration parameter**	$\mathrm{m\,h^{-1}\,^{\circ}C^{-1}}$
a_c	average contact area	variable	–
B	constant governing snow densification	constant	$\mathrm{K^{-1}}$
B_Q	constant governing the mass concentration of suspended snow	constant	$\mathrm{s^{-0.544}}$
b	parameter in firn densification	parameter	–
C	constant governing ice sintering function of T_A	constant	$\mathrm{m^3\,s^{-1}}$
C_0	constant governing ice sintering	constant	$\mathrm{m^3\,s^{-1}}$
C_c, C_d, C_g, C_l	coefficient governing cohesive force, drag, form and lift coefficient	parameter	–
c	constant governing snow densification	constant	$\mathrm{s\,h^{-1}}$
c_H	coefficient influencing the lower boundary height for suspension	constant	$\mathrm{m^{-0.27}\,s^{1.27}}$
D	relative firn density	variable	–
D_0	relative density between first and second stage of firn densification	here treated as constant	–
D_c	close-off density	here treated as constant	–
E_1,E_2,E_3	constants governing the influence of wind in snow densification	constant	$\mathrm{m\,s^{-1}}$
E_{MF}, E_S, E_W	mass flux due to the transformation of snow in firn	variable	$\mathrm{kg\,m^{-2}\,h^{-1}}$
e	melt-freeze factor	**calibration parameter**	–
F	melt freeze mass flux	variable	$\mathrm{kg\,m^{-2}\,h^{-1}}$
g	gravitational acceleration	constant	$\mathrm{m\,s^{-2}}$
H	mountain height	constant	m
h	snowpack height	variable	m
h^*	lower boundary for suspension	variable	m
h_F	firn height	variable	m
h_{MF}	height of ice inside the snowpack	variable	m
h_S	dry snow height	variable	m
h_W	height of water inside the snowpack	variable	m
I, I^*, I_F	multiplicative function	function	

https://doi.org/10.5194/tc-2020-357
Preprint. Discussion started: 21 January 2021

The Cryosphere Discussions

Table B2. List of the symbols used (from K to R)

Symbol	Description	Type	Unit
K	intrinsic permeability of snow	variable	m^2
K_W	intrinsic permeability of water in snow	variable	m^2
k	constant	constant	m
l', l''	firn grain radius in units of the initial radius l	variable	–
M	snow melt mass flux	variable	$\mathrm{kg\,m^{-2}\,h^{-1}}$
M_F	firn mass	variable	$\mathrm{kg\,m^{-2}}$
M_{MF}	mass of ice inside the snowpack	variable	$\mathrm{kg\,m^{-2}}$
M_S	dry snow mass	variable	$\mathrm{kg\,m^{-2}}$
M_W	mass of water inside the snowpack	variable	$\mathrm{kg\,m^{-2}}$
$MAAT$	mean annual air temperature	constant	$^\circ\mathrm{C}$
$MAFT$	mean annual firn temperature	constant	$^\circ\mathrm{C}$
m	parameter governing ice sintering	parameter	–
m_p	slope of the precipitation altitude relationship	parameter	$\mathrm{mm\,d^{-1}\,m^{-1}}$
n	parameter governing ice sintering	parameter	–
O	run-off rate	variable	$\mathrm{kg\,m^{-2}\,h^{-1}}$
O_F	firn melt mass flux	variable	$\mathrm{kg\,m^{-2}\,h^{-1}}$
P	overburden pressure	variable	Pa
P^*	effective stress	variable	Pa
P_b	pressure in the bubbles	variable	Pa
P_c	atmospheric pressure at the close-off	here treated as constant	Pa
P_F	variation of mass due to rain on firn	variable	$\mathrm{kg\,m^{-2}\,h^{-1}}$
P_R	mass flux of liquid precipitation	variable	$\mathrm{kg\,m^{-2}\,h^{-1}}$
P_S	mass flux of solid precipitation	variable	$\mathrm{kg\,m^{-2}\,h^{-1}}$
p	daily precipitation	variable	$\mathrm{mm\,d^{-1}}$
p_r	reconstructed daily liquid precipitation	variable	$\mathrm{mm\,d^{-1}}$
Q	snow erosion	variable	$\mathrm{kg\,m^{-2}\,h^{-1}}$
Q_1, Q_2, Q_s	activation energy	constant	$\mathrm{J\,mol^{-1}}$
Q_{salt}	snow transport in saltation	variable	$\mathrm{kg\,m^{-1}\,s^{-1}}$
Q_{susp}	snow transport in saltation	variable	$\mathrm{kg\,m^{-1}\,s^{-1}}$
R	grain radius	variable	m
R_G	gas constant	constant	$\mathrm{J\,K^{-1}\,mol^{-1}}$
r	liquid precipitation rate	variable	$\mathrm{m\,h^{-1}}$

https://doi.org/10.5194/tc-2020-357
Preprint. Discussion started: 21 January 2021

The Cryosphere Discussions
Open Access
EGU

Table B3. List of the symbols used (from S to Z)

Symbol	Description	Type	Unit
S^*	effective saturation degree of the snowpack	variable	–
S_A	mass of the most recent non eroded snow events	variable	$\mathrm{kg\,m^{-2}\,h^{-1}}$
$\boldsymbol{S_R}$	vector of non eroded snow events	variable	$\mathrm{kg\,m^{-2}\,h^{-1}}$
S_r	average saturation degree of the porous matrix	variable	–
S_{r_i}	irreducible saturation degree	variable	–
SD	observed snow depth	variable	m
SSA	specific surface area	variable	$\mathrm{m^2\,kg^{-1}}$
SWE	snow water equivalent	variable	m
s	solid precipitation rate	variable	$\mathrm{m\,h^{-1}}$
s_w	solid precipitation rate in water equivalent	variable	$\mathrm{mm\,d^{-1}}$
T_0	surface temperature	variable	$^\circ\mathrm{C}$
T_A	air temperature	variable	$^\circ\mathrm{C}$
T_F	average firn temperature	variable	$^\circ\mathrm{C}$
T_S	average snow temperature	variable	$^\circ\mathrm{C}$
T_τ	threshold temperature for melting	here treated as constant	$^\circ\mathrm{C}$
t_d	time since deposition	variable	s
t_i	time instant at the end of water year i	constant	h
U	wind speed contribution to snow densification	variable	$\mathrm{m\,s^{-1}}$
u	10 m wind speed	variable	$\mathrm{m\,s^{-1}}$
u_2	2 m wind speed	variable	$\mathrm{m\,s^{-1}}$
u^*	atmospheric friction velocity	variable	$\mathrm{m\,s^{-1}}$
u_t^*	critical friction velocity	variable	$\mathrm{m\,s^{-1}}$
V_F	firn volume	variable	$\mathrm{m^3}$
V_{MF}	volume of ice inside the snowpack	variable	$\mathrm{m^3}$
V_S	dry snow volume	variable	$\mathrm{m^3}$
V_W	volume of water inside the snowpack	variable	$\mathrm{m^3}$
Z	number of particle contacts	variable	–
Z_0	initial number of particle contacts	constant	–
z	altitude	variable	m
z_0	aerodynamic roughness length	variable	m
z_b	top boundary for suspension	here treated as constant	m
z_M	maximum firn depth influenced by air temperature	here treated as constant	m
z_m	altitude of maximum precipitation	here treated as constant	m
z_r	reference height for mass concentration of suspended snow	constant	m

https://doi.org/10.5194/tc-2020-357
Preprint. Discussion started: 21 January 2021

The Cryosphere
Discussions
Open Access

Table B4. List of the symbols used (Greek letters)

Symbol	Description	Type	Unit
α	constant governing run-off rate	constant	$\mathrm{m^{-1}\,s^{-1}}$
α'	time conversion constant	constant	$\mathrm{s\,h^{-1}}$
Γ	temperature lapse rate	parameter	$\mathrm{^{\circ}C\,m^{-1}}$
γ	parameter function of γ', T_F	parameter	$\mathrm{Pa^{-1}\,h^{-1}}$
γ'	parameter governing firn densification	**calibration parameter**	$\mathrm{Pa^{-1}\,h^{-1}}$
Δt	time step	constant	h
δ	Dirac delta function	function	
η	mass concentration of suspended snow	variable	$\mathrm{kg\,m^{-3}}$
θ_W	volumetric liquid water content	variable	–
κ	von Kármán constant	constant	–
ρ	bulk density of snow	variable	$\mathrm{kg\,m^{-3}}$
ρ_a	atmospheric density	here treated as constant	$\mathrm{kg\,m^{-3}}$
ρ_F	firn density	variable	$\mathrm{kg\,m^{-3}}$
ρ_i	ice density	here treated as constant	$\mathrm{kg\,m^{-3}}$
ρ_{NS}	fresh snow density	variable	$\mathrm{kg\,m^{-3}}$
ρ_S	dry snow density	variable	$\mathrm{kg\,m^{-3}}$
ρ_W	water density	here treated as constant	$\mathrm{kg\,m^{-3}}$
ς	stress due to ice cohesion	variable	Pa
τ_t	critical shear stress for erosion	variable	Pa
ϕ	porosity	variable	–

https://doi.org/10.5194/tc-2020-357
Preprint. Discussion started: 21 January 2021

The Cryosphere Discussions

Author contributions. CDM and FB conceived the model. FB took care of data, and developed the case study. FB wrote a first draft of the manuscript. FB and CDM reviewed the manuscript.

Competing interests. No competing interests are present.

Acknowledgements. We would like to thank ARPA Piemonte for the meteorological data used in this study. Gratitude is also due to Josef Lier for KCC ice core data and to Pascal Bohleber for the information about Colle Gnifetti. One last thank you to Scenari Digitali and Rifugi Monterosa for additional information about Capanna Regina Margherita.

https://doi.org/10.5194/tc-2020-357
Preprint. Discussion started: 21 January 2021

The Cryosphere Discussions

References

Adhikary, S. P.: Inaugural address, in: Snow and glacier hydrology, edited by Young, G. J., p. x, International Association of Hydrological Sciences (IAHS), Wallingford, Oxfordshire OX10 8BB, UK., 1993.

Aizen, V. B., Aizen, E. M., and Melack, J. M.: Precipitation, melt and runoff in the northern Tien Shan, J. Hydrol., 186, 229–251, https://doi.org/10.1016/S0022-1694(96)03022-3, 1996.

Alean, J., Haeberli, W., and Schädler, B.: Snow accumulation, firn temperature and solar radiation in the area of the Colle Gnifetti core drilling site (Monte Rosa, Swiss Alps): distribution patterns and interrelationships, Zeitschrift für Gletscherkunde und Glazialgeologie, 19, 131–147, 1983.

Alley, R. B.: Firn densification by grain-boundary sliding: a first model, J. Phys. Colloques, 48, C1–249–C1–256, https://doi.org/10.1051/jphyscol:1987135, 1987.

Alpert, P.: Mesoscale Indexing of the Distribution of Orographic Precipitation over High Mountains, J. Climate Appl. Meteor., 25, 532–545, https://doi.org/10.1175/1520-0450(1986)025<0532:MIOTDO>2.0.CO;2, 1986.

Anderson, E. A.: A point energy and mass balance model of a snow cover, vol. 19, NOAA Technical Report NWS, 1976.

Ardenghi, N.: Geochemical characterization of a shallow firn core retrieved from Colle Gnifetti (Monte Rosa, Italy), Master's thesis, Università Ca' Foscari Venezia, Italy, 2012.

Arnaud, L., Barnola, J. M., and Duval, P.: Physical modeling of the densification of snow/firn and ice in the upper part of polar ice sheets, in: Physics of ice core records, edited by Hondoh, T., pp. 285–305, Hokkaido University Press, Sapporo, Japan, 2000., 2000.

Arthern, R. J., Vaughan, D. G., Rankin, A. M., Mulvaney, R., and Thomas, E. R.: In situ measurements of Antarctic snow compaction compared with predictions of models, J. Geophys. Res.-Earth, 115, https://doi.org/10.1029/2009JF001306, 2010.

Arzt, E.: The influence of an increasing particle coordination on the densification of spherical powders, Acta Metall. Mater., 30, 1883–1890, https://doi.org/10.1016/0001-6160(82)90028-1, 1982.

Arzt, E., Ashby, M. F., and Easterling, K. E.: Practical applications of hotisostatic pressing diagrams: four case studies, Metall. Mater. Trans. A, 14, 211–221, https://doi.org/10.1007/BF02651618, 1983.

Avanzi, F., De Michele, C., Ghezzi, A., Jommi, C., and Pepe, M.: A processing- modeling routine to use SNOTEL hourly data in snowpack dynamic models, Adv. Water Resour., 73, 16–29, https://doi.org/10.1016/j.advwatres.2014.06.011, 2014.

Avanzi, F., Yamaguchi, S., Hirashima, H., and De Michele, C.: Bulk volumetric liquid water content in a seasonal snowpack: modeling its dynamics in different climatic conditions, Adv. Water Resour., 86, 1–13, https://doi.org/10.1016/j.advwatres.2015.09.021, 2015.

Bader, H.: Sorge's Law of densification of snow on high polar glaciers, J. Glaciol., 2, 319–323, https://doi.org/10.3189/S0022143000025144, 1954.

Benn, D. I. and Evans, D. J. A.: Glaciers and glaciation (Second edition), Hodder Education, London, 2010.

Bohleber, P., Wagenbach, D., Schöner, W., and Böhm, R.: To what extent do water isotope records from low accumulation Alpine ice cores reproduce instrumental temperature series?, Tellus B, 65, 20 148, https://doi.org/10.3402/tellusb.v65i0.20148, 2013.

Bohleber, P., Erhardt, T., Spaulding, N., Hoffmann, H., Fischer, H., and Mayewski, P.: Temperature and mineral dust variability recorded in two low-accumulation Alpine ice cores over the last millennium, Clim. Past, 14, 21–37, https://doi.org/10.5194/cp-14-21-2018, 2018.

Bréant, C., Martinerie, P., Orsi, A., Arnaud, L., and Landais, A.: Modelling firn thickness evolution during the last deglaciation: constraints on sensitivity to temperature and impurities, Clim. Past, 13, 833–853, https://doi.org/10.5194/cp-13-833-2017, 2017.

https://doi.org/10.5194/tc-2020-357
Preprint. Discussion started: 21 January 2021

The Cryosphere Discussions

Calonne, N., Geindreau, C., Flin, F., Morin, S., Lesaffre, B., Rolland Du Roscoat, S., and Charrier, P.: 3-D image-based numerical computations of snow permeability: links to specific surface area, density, and microstructural anisotropy, Cryosphere, 6, 939–951, https://doi.org/10.5194/tc-6-939-2012, 2012.

Colbeck, S.: A theory of water percolation in snow, Journal of glaciology, 11, 369–385, https://doi.org/10.3189/S0022143000022346, 1972.

Cuffey, K. M. and Paterson, W. S. B.: The physics of glaciers (Fourth edition), Butterworth Heinemann-Elsevier, Burlington, 2010.

De Michele, C., Avanzi, F., Ghezzi, A., and Jommi, C.: Investigating the dynamics of bulk snow density in dry and wet conditions using a one-dimensional model, Cryosphere, 7, 433–444, https://doi.org/10.5194/tc-7-433-2013, 2013.

Déry, S. J. and Taylor, P. A.: Some aspects of the interaction of blowing snow with the atmospheric boundary layer, Hydrol. Process., 10, 1345–1358, https://doi.org/10.1002/(SICI)1099-1085(199610)10:10<1345::AID-HYP465>3.0.CO;2-2, 1996.

DeWalle, D. R. and Rango, A.: Principles of snow hydrology, Cambridge University Press, New York, 2008.

Domine, F., Taillandier, A.-S., and Simpson, W. R.: A parameterization of the specific surface area of seasonal snow for field use and for models of snowpack evolution, J. Geophys. Res.-Earth, 112, https://doi.org/10.1029/2006JF000512, 2007.

Doyle, S. H., Hubbard, A., Van De Wal, R. S., Box, J. E., Van As, D., Scharrer, K., Meierbachtol, T. W., Smeets, P. C., Harper, J. T., and Johansson, E.: Amplified melt and flow of the Greenland ice sheet driven by late-summer cyclonic rainfall, Nat. Geosci., 8, 647–653, https://doi.org/10.1038/ngeo2482, 2015.

Duan, Q., Sorooshian, S., and Gupta, V.: Effective and efficient global optimization for conceptual rainfall-runoff models, Water Resour. Res., 28, 1015–1031, https://doi.org/10.1029/91WR02985, 1992.

Duan, Q. Y., Gupta, V. K., and Sorooshian, S.: Shuffled complex evolution approach for effective and efficient global minimization, J. of Optimiz. Theory App., 76, 501–521, https://doi.org/10.1007/BF00939380, 1993.

Eichler, A., Schwikowski, M., Gäggeler, H. W., Furrer, V., Synal, H.-A., Beer, J., Saurer, M., and Funk, M.: Glaciochemical dating of an ice core from upper Grenzgletscher (4200 m a.s.l.), J. Glaciol., 46, 507–515, https://doi.org/10.3189/172756500781833098, 2000.

Fountain, A. G. and Tangborn, W. V.: The Effect of Glaciers on Streamflow Variations, Water Resour. Res., 21, 579–586, https://doi.org/10.1029/WR021i004p00579, 1985.

Gäggeler, H., von Gunten, H. R., Rössler, E., Oeschger, H., and Schotterer, U.: 210 Pb dating of Cold Alpine Firn/Ice Cores From Colle Gnifetti, Switzerland, J. Glaciol., 29, 165–177, https://doi.org/10.3189/2014AoG66A151, 1983.

Haeberli, W. and Alean, J.: Temperature and accumulation of high altitude firn in the Alps, Ann. Glaciol., 6, 161–163, https://doi.org/10.3189/1985AoG6-1-161-163, 1985.

Haeberli, W. and Funk, M.: Borehole temperatures at the Colle Gnifetti core-drilling site (Monte Rosa, Swiss Alps), J. Glaciol., 37, 37–46, https://doi.org/10.3189/S0022143000042775, 1991.

Hagg, W., Braun, L. N., Kuhn, M., and Nesgaard, T. I.: Modelling of hydrological response to climate change in glacierized Central Asian catchments, J. Hydrol., 332, 40–53, https://doi.org/10.1016/j.jhydrol.2006.06.021, 2007.

He, S. and Ohara, N.: A New Formula for Estimating the Threshold Wind Speed for Snow Movement, J. Adv. Model. Earth Sy., 9, 2514–2525, https://doi.org/10.1002/2017MS000982, 2017.

Henn, B., Raleigh, M. S., Fisher, A., and Lundquist, J. D.: A comparison of methods for filling gaps in hourly near-surface air temperature data, J. Hydrometeorol., 14, 929–945, https://doi.org/10.1175/JHM-D-12-027.1, 2013.

Herron, M. M. and Langway, C. C.: Firn Densification: An Empirical Model, J. Glaciol., 25, 373–385, https://doi.org/10.1017/S0022143000015239, 1980.

https://doi.org/10.5194/tc-2020-357
Preprint. Discussion started: 21 January 2021

Hock, R.: Temperature index melt modelling in mountain areas, J. Hydrol., 282, 104–115, https://doi.org/10.1016/S0022-1694(03)00257-9, 2003.

Hock, R., Jansson, P., and Braun, L. N.: Modelling the response of mountain glacier discharge to climate warming, in: Global Change and Mountain Regions, edited by Huber, U., Bugmann, H., and M.A., R., vol. 23 of *Advances in Global Change Research*, pp. 243–252, Springer, Dordrecht, 2005.

Hock, R., Rasul, G., Adler, C., Cáceres, B., Gruber, S., Hirabayashi, Y., Jackson, M., Kääb, A., Kang, S., Kutuzov, S., Milner, A., Molau, U., Morin, S., Orlove, B., and Steltzer, H.: High Mountain Areas, in: IPCC Special Report on the Ocean and Cryosphere in a Changing Climate, edited by Pörtner, H.-O., Roberts, D. C., Masson-Delmotte, V., Zhai, P., Tignor, M., Poloczanska, E., Mintenbeck, K., Alegría, A., Nicolai, M., Okem, A., Petzold, J., Rama, B., and Weyer, N. M., In press, 2019.

Hosler, C. L., Jensen, D. C., and Goldshlak, L.: On the aggregation of ice crystals to form snow, J. Meteor., 14, 415–420, https://doi.org/10.1175/1520-0469(1957)014<0415:OTAOIC>2.0.CO;2, 1957.

Huss, M.: Density assumptions for converting geodetic glacier volume change to mass change, Cryosphere, 7, 877–887, https://doi.org/10.5194/tc-7-877-2013, 2013.

Huss, M., Jouvet, G., Farinotti, D., and Bauder, A.: Future high-mountain hydrology: a new parameterization of glacier retreat, Hydrol. Earth Syst. Sc., 14, 815–829, https://doi.org/10.5194/hess-14-815-2010, 2010.

Jacka, T. and Jun, L.: The steady-state crystal size of deforming ice, Ann. Glaciol., 20, 13–18, https://doi.org/10.3189/1994AoG20-1-13-18, 1994.

Jansson, P., Hock, R., and Schneider, T.: The concept of glacier storage: a review, J. Hydrol., 282, 116–129, https://doi.org/10.1016/S0022-1694(03)00258-0, 2003.

Jennings, K. S., Winchell, T. S., Livneh, B., and Molotch, N. P.: Spatial variation of the rain-snow temperature threshold across the Northern Hemisphere, Nat. Commun., 9, 1148, https://doi.org/10.1038/s41467-018-03629-7, 2018.

Jost, G., Moore, R. D., Menounos, B., and Wheate, R.: Quantifying the contribution of glacier runoff to streamflow in the upper Columbia River Basin, Canada, Hydrol. Earth Syst. Sc., 16, 849–860, https://doi.org/10.5194/hess-16-849-2012, 2012.

Keck, L.: Climate significance of stable isotope records from Alpine ice cores, Ph.D. thesis, Institute of Environmental Physics, Heidelberg University, Germany, 2001.

Keenan, E., Wever, N., Dattler, M., Lenaerts, J., Medley, B., Kuipers Munneke, P., and Reijmer, C.: Physics-based modeling of Antarctic snow and firn density, The Cryosphere Discussions, 2020, 1–25, https://doi.org/10.5194/tc-2020-175, 2020.

Kelleners, T., Chandler, D., McNamara, J. P., Gribb, M. M., and Seyfried, M.: Modeling the water and energy balance of vegetated areas with snow accumulation, Vadose Zone J., 8, 1013–1030, https://doi.org/10.2136/vzj2008.0183, 2009.

Li, L. and Pomeroy, J. W.: Estimates of Threshold Wind Speeds for Snow Transport Using Meteorological Data, J. Appl. Meteorol., 36, 205–213, https://doi.org/10.1175/1520-0450(1997)0362.0.CO;2, 1997.

Licciulli, C., Bohleber, P., Lier, J., Gagliardini, O., Hoelzle, M., and Eisen, O.: A full Stokes ice-flow model to assist the interpretation of millennial-scale ice cores at the high-Alpine drilling site Colle Gnifetti, Swiss/Italian Alps, J. Glaciol., 66, 35–48, https://doi.org/10.1017/jog.2019.82, 2020.

Liston, G. E. and Elder, K.: A meteorological distribution system for high-resolution terrestrial modeling (MicroMet), J. Hydrometeorol., 7, 217–234, https://doi.org/10.1175/JHM486.1, 2006.

Liston, G. E., Haehnel, R. B., Sturm, M., Hiemstra, C. A., Berezovskaya, S., and Tabler, R. D.: Simulating complex snow distributions in windy environments using SnowTran-3D, J. Glaciol., 53, 241–256, https://doi.org/10.3189/172756507782202865, 2007.

Luo, Y., Arnold, J., Liu, S., Wang, X., and Chen, X.: Inclusion of glacier processes for distributed hydrological modeling at basin scale with application to a watershed in Tianshan Mountains, northwest China, J. Hydrol., 477, 72–85, https://doi.org/10.1016/j.jhydrol.2012.11.005, 2013.

Lüthi, M. and Funk, M.: Dating ice cores from a high Alpine glacier with a flow model for cold firn, Ann. Glaciol., 31, 69–79, https://doi.org/10.3189/172756400781820381, 2000.

Maeno, N. and Arakawa, M.: Adhesion shear theory of ice friction at low sliding velocities, combined with ice sintering, J. Appl. Phys., 95, 134–139, https://doi.org/10.1063/1.1633654, 2004.

Mariani, I., Eichler, A., Jenk, T. M., Brönnimann, S., Auchmann, R., Leuenberger, M., and Schwikowski, M.: Temperature and precipitation signal in two Alpine ice cores over the period 1961–2001, Clim. Past, 10, 1093–1108, https://doi.org/10.5194/cp-10-1093-2014, 2014.

Martorina, S., Olivero, A., Loglisci, N., Pelosini, R., and Paesano, G.: Capanna Margherita - The highest meteorological station in Europe. Is it possible to consider it as representative of synoptic weather?, in: International Conference on Alpine Meteorology and MAP-Meeting, Brig, Switzerland, 2003.

Naz, B. S., Frans, C. D., Clarke, G., Burns, P. J., and Lettenmaier, D. P.: Modeling the effect of glacier recession on streamflow response using a coupled glacio–hydrological model, Hydrol. Earth Syst. Sc., 18, 787–802, https://doi.org/10.5194/hess-18-787-2014, 2014.

Pomeroy, J. and Male, D.: Steady-state suspension of snow, J. Hydrol., 136, 275–301, https://doi.org/10.1016/0022-1694(92)90015-N, 1992.

Pomeroy, J. W. and Gray, D. M.: Saltation of snow, Water Resour. Res., 26, 1583–1594, https://doi.org/10.1029/WR026i007p01583, 1990.

Pomeroy, J. W., Gray, D. M., and Landine, P. G.: The Prairie Blowing Snow Model: characteristics, validation, operation, J. Hydrol., 144, 165–192, https://doi.org/10.1016/0022-1694(93)90171-5, 1993.

Pomeroy, J. W., Marsh, P., and Gray, D. M.: Application of a distributed blowing snow model to the Arctic, Hydrol. Process., 11, 1451–1464, https://doi.org/doi: 10.1002/(SICI)1099-1085(199709)11:113.0.CO;2-Q; 10, 1997.

Roe, G. H.: Orographic precipitation, Annu. Rev. Earth Pl. Sc., 33, 645–671, https://doi.org/10.1146/annurev.earth.33.092203.122541, 2005.

Schöner, Schöner, W., Auer, I., Böhm, R., Keck, L., and Wagenbach, D.: Spatial representativity of air-temperature information from instrumental and ice-core-based isotope records in the European Alps, Ann. Glaciol., 35, 157–161, https://doi.org/10.3189/172756402781816717, 2002.

Seibert, J., Vis, M. J. P., Kohn, I., Weiler, M., and Stahl, K.: Technical note: Representing glacier geometry changes in a semi-distributed hydrological model, Hydrol. Earth Syst. Sc., 22, 2211–2224, https://doi.org/10.5194/hess-22-2211-2018, 2018.

Sigl, M., Abram, N. J., Gabrieli, J., Jenk, T. M., Osmont, D., and Schwikowski, M.: Record of black carbon (rBC), bismuth, lead and others from 1741 to 2015 AD from Colle Gnifetti ice cores GC15 and GC03B (Swiss/Italian Alps), PANGAEA, https://doi.org/10.1594/PANGAEA.894787, in supplement to: Sigl, M et al. (2018): 19th century glacier retreat in the Alps preceded the emergence of industrial black carbon deposition on high-alpine glaciers. Cryosphere, 12, 3311–3331, https://doi.org/10.5194/tc-12-3311-2018, 2018.

Smiraglia, C., Maggi, V., Novo, A., Rossi, G., and Johnston, P.: Preliminary results of two ice core drillings on Monte Rosa (Colle Gnifetti and Colle del Lys), Italian Alps, Geogr. Fis. Din. Quat., 23, 165–172, 2000.

Suter, S., Laternser, M., Haeberli, W., Frauenfelder, R., and Hoelzle, M.: Cold firn and ice of high-altitude glaciers in the Alps: measurements and distribution modelling, J. Glaciol., 47, 85–96, https://doi.org/10.3189/172756501781832566, 2001.

Vaughan, D. G., Comiso, J. C., Allison, I., Carrasco, J., Kaser, G., Kwok, R., Mote, P., Murray, T., Paul, F., Ren, J., Rignot, E., Solomina, O., Steffen, K., and Zhang, T.: Observations: Cryosphere, in: Climate Change 2013: The Physical Science Basis. Contribution of Working Group I to the Fifth Assessment Report of the Intergovernmental Panel on Climate Change, edited by Stocker, T. F., Qin, D., Plattner,

https://doi.org/10.5194/tc-2020-357
Preprint. Discussion started: 21 January 2021

G.-K., Tignor, M., Allen, S. K., Boschung, J., Nauels, A., Xia, Y., Bex, V., and Midgley, P. M., Cambridge University Press, Cambridge, United Kingdom and New York, NY, USA, 2013.

Vionnet, V., Guyomarc'h, G., Lafaysse, M., Naaim-Bouvet, F., Giraud, G., and Deliot, Y.: Operational implementation and evaluation of a blowing snow scheme for avalanche hazard forecasting, Cold Reg. Sci. Technol., 147, 1–10, https://doi.org/10.1016/j.coldregions.2017.12.006, 2018.

Wagenbach, D., Münnich, K., Schotterer, U., and Oeschger, H.: The anthropogenic impact on snow chemistry at Colle Gnifetti, Swiss Alps, Ann. Glaciol,, 10, 183–187, https://doi.org/10.3189/S0260305500004407, 1988.

Wagenbach, D., Bohleber, P., and Preunkert, S.: Cold, alpine ice bodies revisited: what may we learn from their impurity and isotope content?, Geogr. Ann. A, 94, 245–263, https://doi.org/10.1111/j.1468-0459.2012.00461.x, 2012.

Wilkinson, D. S. and Ashby, M. F.: Pressure sintering by power law creep, Acta Metall. Mater., 23, 1277–1285, https://doi.org/10.1016/0001-6160(75)90136-4, 1975.

Wortmann, M., Bolch, T., Su, B., and Krysanova, V.: An efficient representation of glacier dynamics in a semi-distributed hydrological model to bridge glacier and river catchment scales, J. Hydrol., 573, 136–152, https://doi.org/10.1016/j.jhydrol.2019.03.006, 2019.